A detailed analysis of some local earthquakes at Somma-Vesuvius

Paolo Capuano ([1]), **Ugo Coppa** ([1]), **Giuseppe De Natale** ([1]), **Felice Di Sena** ([1]), **Cataldo Godano** ([1]) **and Claudia Troise** ([1])([2])

([1]) *Osservatorio Vesuviano, Napoli, Italy*

([2]) *Dipartimento di Geofisica e Vulcanologia, Università di Napoli «Federico II», Napoli, Italy*

Abstract

In this paper, we analyze local earthquakes which occurred at Somma-Vesuvius during two episodes of intense seismic swarms, in 1989 and 1995 respectively. For the selected earthquakes we have computed accurate hypocentral locations, focal mechanisms and spectral parameters. We have also studied the ground acceleration produced by the largest events of the sequences ($M_L > 3.0$), at various digital stations installed in the area during the periods of higher seismic activity. The main result is that seismicity during the two swarm episodes presents similar features in both locations and focal mechanisms. Strong site dependent effects are evidenced in the seismic radiation and strong amplifications in the frequency band 10-15 Hz are evident at stations located on the younger Vesuvius structure, with respect to one located on the ancient Somma structure. Furthermore, seismic stations show peak accelerations for the same events of more than one order of magnitude apart.

Key words *Somma-Vesuvius – seismicity – focal mechanisms – spectral analysis*

1. Introduction

Mount Vesuvius is a strato-volcano consisting of a volcanic cone (Gran Cono) built within a summit caldera (Mt. Somma). It is located in a densely populated (about 700 000 inhabitans) and noisy area. The Somma-Vesuvius complex has been formed over the last 25 000 years by successive eruptions of variable explosiveness, ranging from the quiet lava outpourings, that characterize much of the latest activity, to the explosive Plinian eruptions, including the one that destroyed Pompei in 79 A.D., alternated with long quiescent periods. Current structural models are extrapolated from the knowledge, unfortunately poor, about the shallow crustal structure beneath the volcano. At present, the main information comes from a seismic reflection survey carried out in 1973 in the Bay of Naples (Finetti and Morelli, 1974), from a deep drilling (Trecase well) carried out for geothermal purposes (Principe *et al.*, 1987), from a 2D modelling of gravity and aeromagnetic anomalies (Cassano and La Torre, 1987) and from a *PmP* phase detected by a deep seismic sounding (Ferrucci *et al.*, 1989).

Currently, Mt. Vesuvius is characterized by a low energy seismicity (Berrino *et al.*, 1993; Vilardo *et al.*, 1996); local earthquakes occur at an average rate of some hundreds per year, in the magnitude range $0 < M_L < 3.4$. Seismic activity is the only indicator of the internal dynamics of this quiescent volcano. The study of local seismicity at Vesuvius has many implications for the determination of the shallow crustal structure of the volcanic area, putting constraints on the stress field of the area and improving the knowledge of the 3D velocity distribution.

Mailing address: Dr. Paolo Capuano, Osservatorio Vesuviano, Via A. Manzoni, 249, 80123 Napoli, Italy; e-mail: capuano@osve.unina.it

The aim of this paper is to present a first attempt to evaluate the peculiarity of seismicity occurring at Somma-Vesuvius during swarm episodes and to evaluate the peak ground motion, produced by local earthquakes, linked to local site amplification, that is very important in the assessment of seismic hazard in such a densely populated area.

2. Earthquake locations in 3D

Recently, a 2D and a preliminary 3D velocity model have been obtained for the Somma Vesuvius area, based on the combined analysis of shot data on a seismic profile performed in 1994 (Zollo *et al.*, 1996, 1998) and earthquake data (De Natale *et al.*, 1998). The 3D velocity model obtained by De Natale *et al.* (1998) was used in this paper to obtain earthquakes location. Earthquake locations were obtained using the Thurber (1983) inversion program, with the ART2 ray tracing algorithm. Figure 1 shows, across a W-E section of the velocity model, a set of about 200 earthquake locations. The peculiar feature of such a velocity model is the presence of a high velocity zone centered along the crater axis, going down to more than 5 km in depth.

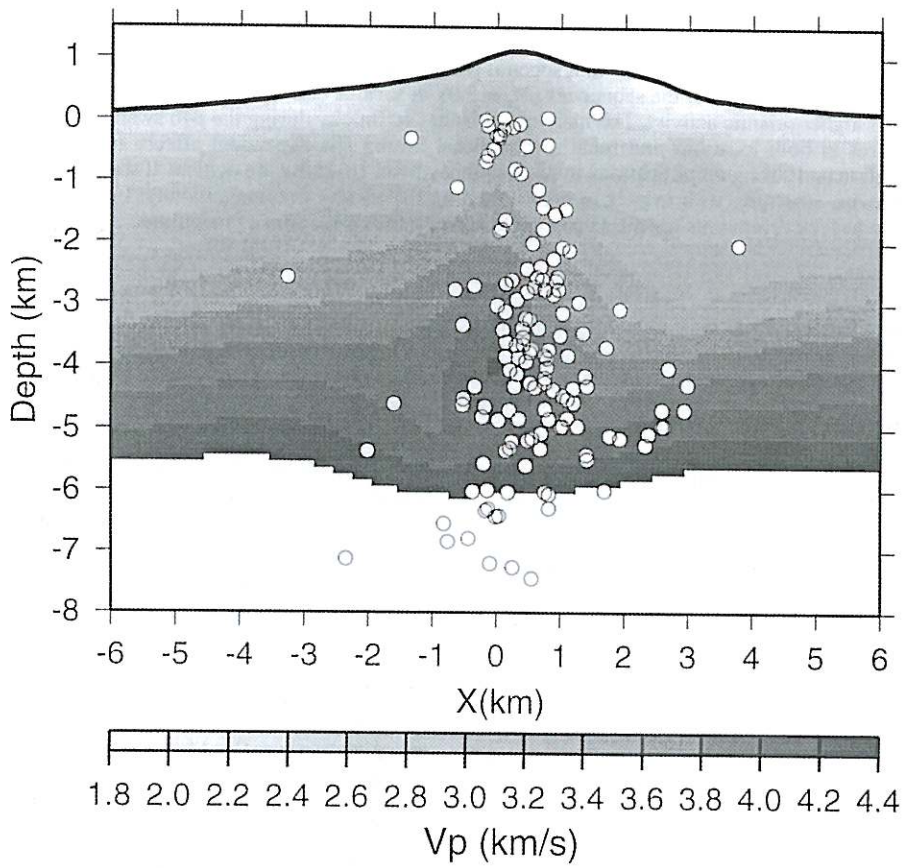

Fig. 1. W-E section, crossing the Gran Cono, showing the *P*-velocity model used for earthquake location. Note the high velocity zone centered along the crater axis. Hypocentral locations of a set of about 200 earthquakes are shown superimposed on the velocity model.

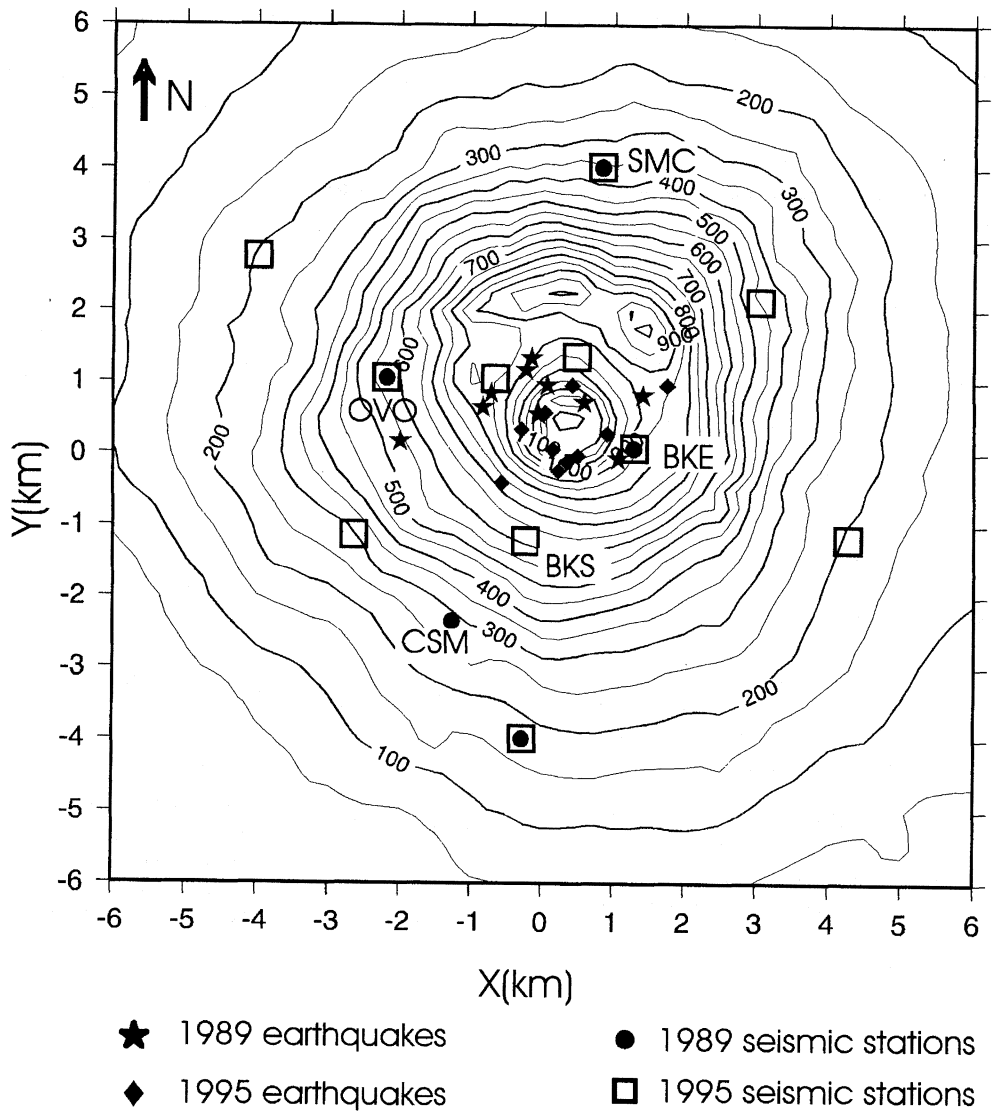

Fig. 2. Elevation (meters) contour map of Vesuvius with superimposed the seismic station operating during the seismic swarm of 1989 and 1995. Some epicentral locations are also shown.

Such a zone is marked by positive, high V_p and V_s velocity anomalies. Seismicity is strongly concentrated within the high velocity anomaly, with depth in the range from –1 km (within the volcanic edifice) to 5-6 km. Some earthquake locations of the 1989 episode of increased seismicity are shown in fig. 2. For earthquakes belonging to this episode, the recording network, shown in fig. 2, consisted of one analog stations located within 3 km from the crater,

and 4 additional three component digital stations. The largest earthquake which occurred in this period was the M_L = 3.2 event (89/03/19 20:22).

In the period August-September 1995, a new episode of a large increase in seismicity occurred. The seismic network considered here consisted of 10 analog stations (within a radius of 10 km from the crater) of the Vesuvius network, some of them equipped with three component sensors, and one three component digital station (fig. 2). The locations of 10 earthquakes which occurred in the period August-September 1995 are shown in fig. 2.

The largest events which occurred in this period are the M_L = 3.2 event (95/09/16 11:03) and the M_L = 3.1 event (95/09/24 03:26).

3. Focal mechanism determination

The analysis of earthquake focal mechanisms represents an important tool for the determination of the seismogenic mechanisms at Mt. Vesuvius. In this study we adopted a Bayesian method, utilising different data sets: first *P* wave polarities, *S* wave polarisation directions and *S/P* amplitude ratios. Such data can be inverted both in terms of double couple mechanisms, and of other kinds of volcanic sources (tensile cracks, CLVD, etc.). The variety of data sets, differently from the use of only *P* wave polarity as in classical methods, helps to constrain focal mechanisms also with a small number of recording stations.

3.1. *Method*

The method used for focal mechanism determination was developed by De Natale *et al.* (1991) (see also Zollo and Bernard, 1991; De Natale, 1994). It is based on the Bayesian estimation of the probability density function on the parameter space (m), from a data set (d) formed by polarities of first *P* waves, polarisations of direct *S* waves and *S/P* wave amplitude ratios. The parameter space is formed by all the possible combinations of the three angles defining a double couple mechanism: strike (ϕ), dip (δ) and slip (λ). The parameter space is sampled over a grid with given steps for each parameter, and the probability density at each grid point is computed by the Bayes theorem

P-wave polarity

$$P(d_1|m) \propto \prod_{i=1}^{N_1}\left[1+\Psi\left(R_i^P,\gamma_i,\rho_i\right)\right]\frac{\rho_i}{2}$$

where $\Psi = (1-2\gamma_i)$ erf $(|r_i R_i^P|)$ and erf( ) is the error function, R_i^P is theoretical *P* wave amplitude, γ_i and ρ_i are parameters which controls the range of probability variation around the focal planes.

S-wave polarization direction

$$P(d_2|m) = \prod_{i=1}^{N_2} P(s_i|m) \propto$$

$$\propto \exp\left[-\sum_{i=1}^{N_2}\frac{(s_i - s_i')\omega_i^2}{\sigma_0^2}\right]\times\prod_{i=1}^{N_2}\mathrm{erf}\left(|k_s R_i^s|\right)$$

where $(s_i - s_i')$ is the angular difference between the observed and theoretical *S* vector at the i-th station, ω_i is a weighting factor, σ_0^2 is the variance which accounts for errors in the model and the data R_i^s is the theoretical *S* wave amplitude and k_s is the parameter which controls the shape of erf( ) function; this term weights for the *S* wave amplitude expected at that point from the given mechanism.

Amplitude ratio S/P

$$P(d_3|m) = \prod_{i=1}^{N_3} P(r_i|m) \propto$$

$$\propto \prod_{i=1}^{N_3} F(r_i, r_i', a_i, \tau_i)\times\prod_{i=1}^{N_3}\mathrm{erf}\left(k_r r_i\right)$$

where r_i and r_i' are the theoretical and the observed *S/P* amplitude ratios; a_i is the half-amplitude of the probability density function in the flat region. Out of the region the function decay with Gaussian shape (standard deviation τ).

3.2. *Data analysis*

The described probability method has been applied to determine 15 focal mechanisms of microearthquakes. Given the small number of recording stations, the probability method offers the advantage of using additional data contained in the digital, three component recordings, with respect to classical first *P* pulse amplitudes. In order to clearly show the improvements obtained with this technique we present the example of a $M_L = 2.4$ microearthquake of the 1989 swarm. Figure 3 shows the seismograms recorded at three out of a total of four digital stations and an analog one. Seismograms were filtered between 1 and 6 Hz; the time window for *S* wave analysis is also indicated. For this event, we show the best focal mechanism computed using *P* polarities, *S* polarisations and *S/P* amplitude ratios. Going from fig. 4a to fig. 4c, we can see how the probability density distributions become more and more focused around the best solution, adding to the first *P* wave polarities (a) a set of four *S* wave polarisations (b) and, finally also three *S/P* amplitude ratios (c) computed from the seismograms shown in fig. 3. Parameters used to specify the probability functions are detailed in the following.

For *P* wave polarities: $\rho_i = \rho = 6$, corresponding to a tolerance of about 10° around the nodal planes; $\gamma_i = \gamma = 0.001$. For *S* wave polarisations: standard deviation $\sigma_0 = 15°$. For *S/P* amplitude ratios, $\rho_1 = 8$, $a_1 = 5$, $\tau_1 = 0.5$, $\rho_2 = 11$, $a_2 = 6$, $\tau_2 = 0.5$; this range of variability contains possible unknown variations of Q_s and Q_p, down to

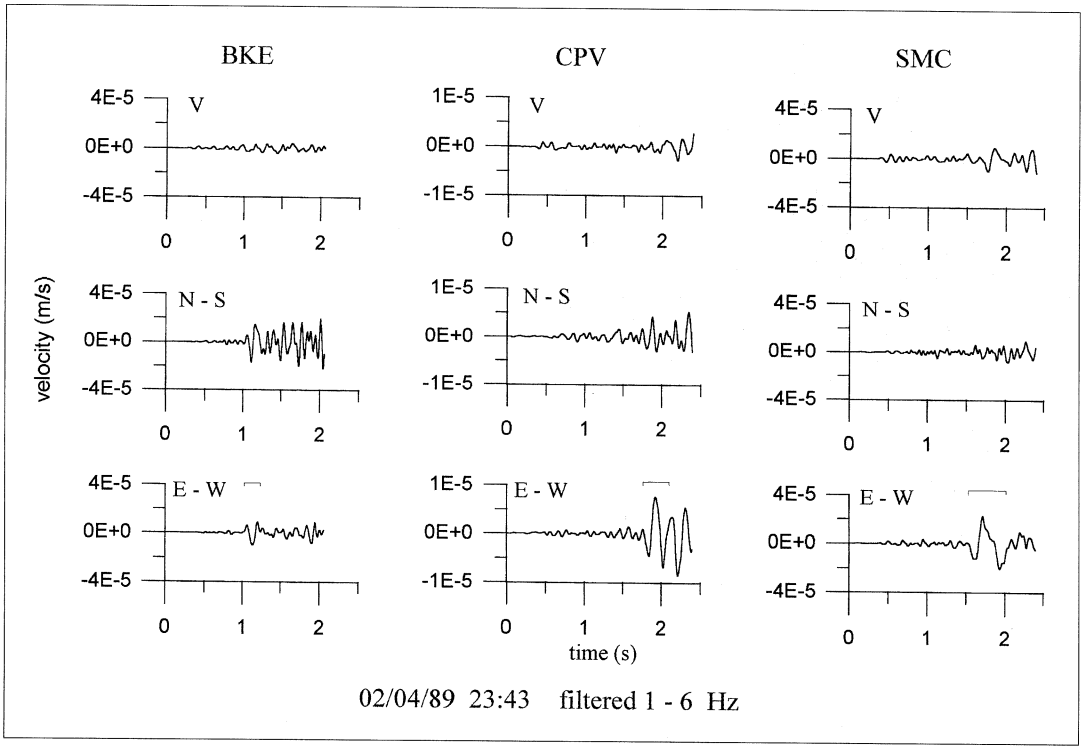

Fig. 3. Seismograms recorded at three (BKE, CPV, SMC) out of a total of four digital stations for an event of $M_L = 2.4$. Seismograms were filtered between 1 and 6 Hz; the time window for *S* wave analysis is also indicated on the E-W components.

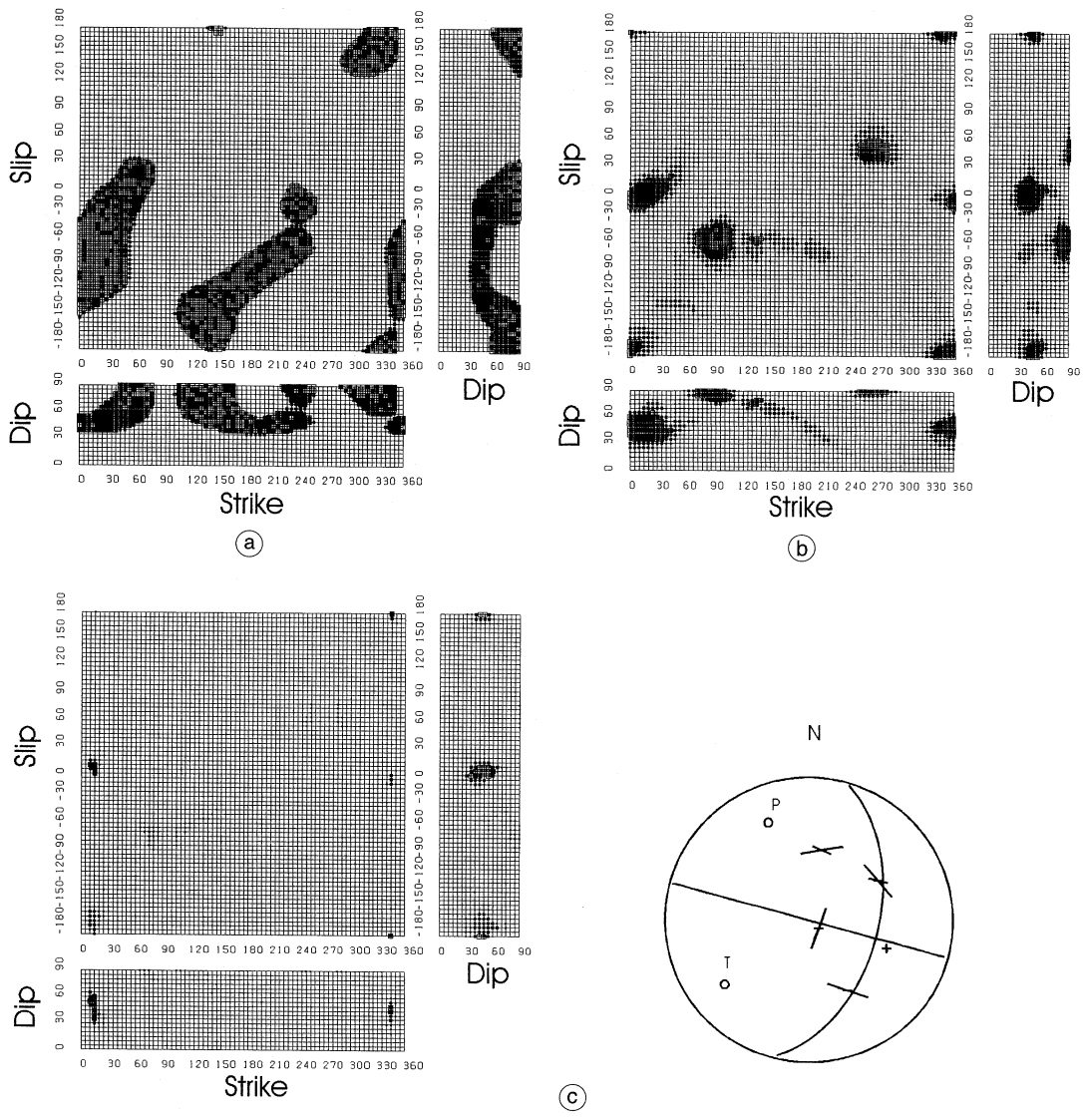

Fig. 4a-c. Example of focal mechanism determination using the probabilistic approach for the earthquake shown in fig. 3. The figure shows the probability density distribution on the focal mechanism parameters (strike, dip and slip) obtained with: a) *P*-wave polarity; b) *P*-wave polarity and *S*-wave polarisations, c) *P* polarity, *S* polarisations and *S/P* amplitude ratios. The mechanism obtained by joint inversion of the three kinds of data is very well constrained, while the one obtained with only *P* polarities is completely undetermined. The stereographic projection (lower hemisphere) shows the maximum likelihood mechanism; observed and computed *P* polarities and *S* polarisations are also projected on the focal sphere. Each rectangle represents one of the three couples of the parameter space, formed by the independent couples of parameters. On each plane symbols for all the values of the third parameter are projected. Large symbols indicate points belonging to the 66% probability level. Intermediate size symbols indicate points belonging to the 90% probability level; small symbols indicate the 99% level.

values of $Q_s = Q_p = 50$ (see also De Natale *et al.*, 1991; De Natale, 1994).

The very large improvement achieved in the focal mechanism determination by the addition of *S* polarisation and *S/P* amplitude ratios to the first *P* wave polarities extend the possibility to compute a focal mechanism even for an event recorded by only five stations. We computed focal mechanisms for the set of fifteen earthquakes belonging to the 1989 and 1995 seismic swarms. The focal mechanisms are shown in fig. 5, together with some mechanisms computed, using the same methods, for earthquakes which occurred in periods of background seismicity from 1987 to 1994 (Vilardo *et al.*, 1996). No marked differences are found in focal mech-

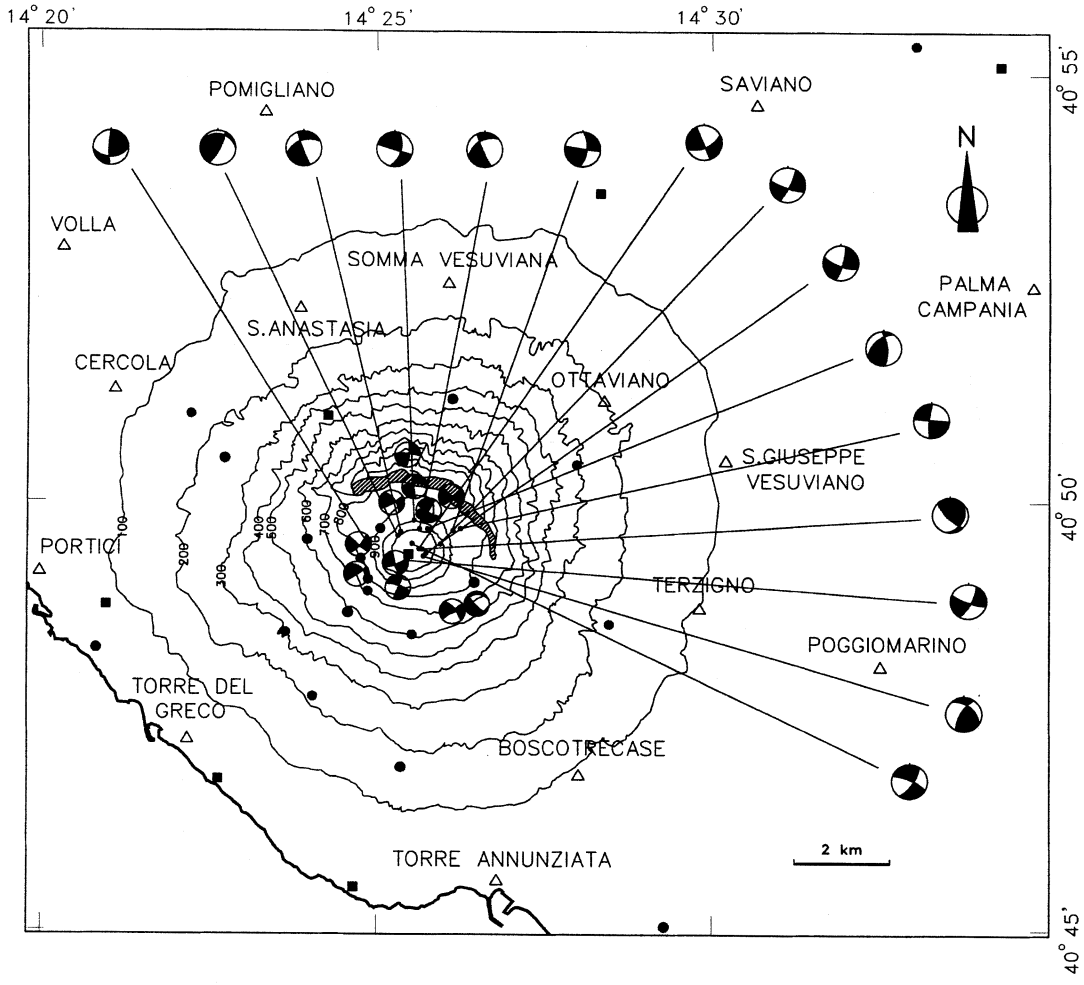

Fig. 5. Map of the Somma-Vesuvius area, showing 15 focal mechanisms of local earthquakes obtained using the probability method. The maximum likelihood solutions are shown. Note the variety of solutions, with a predominance of strike slip component. In the central part of the map examples of focal mechanism for earthquakes occurring during periods of normal background seismicity are shown.

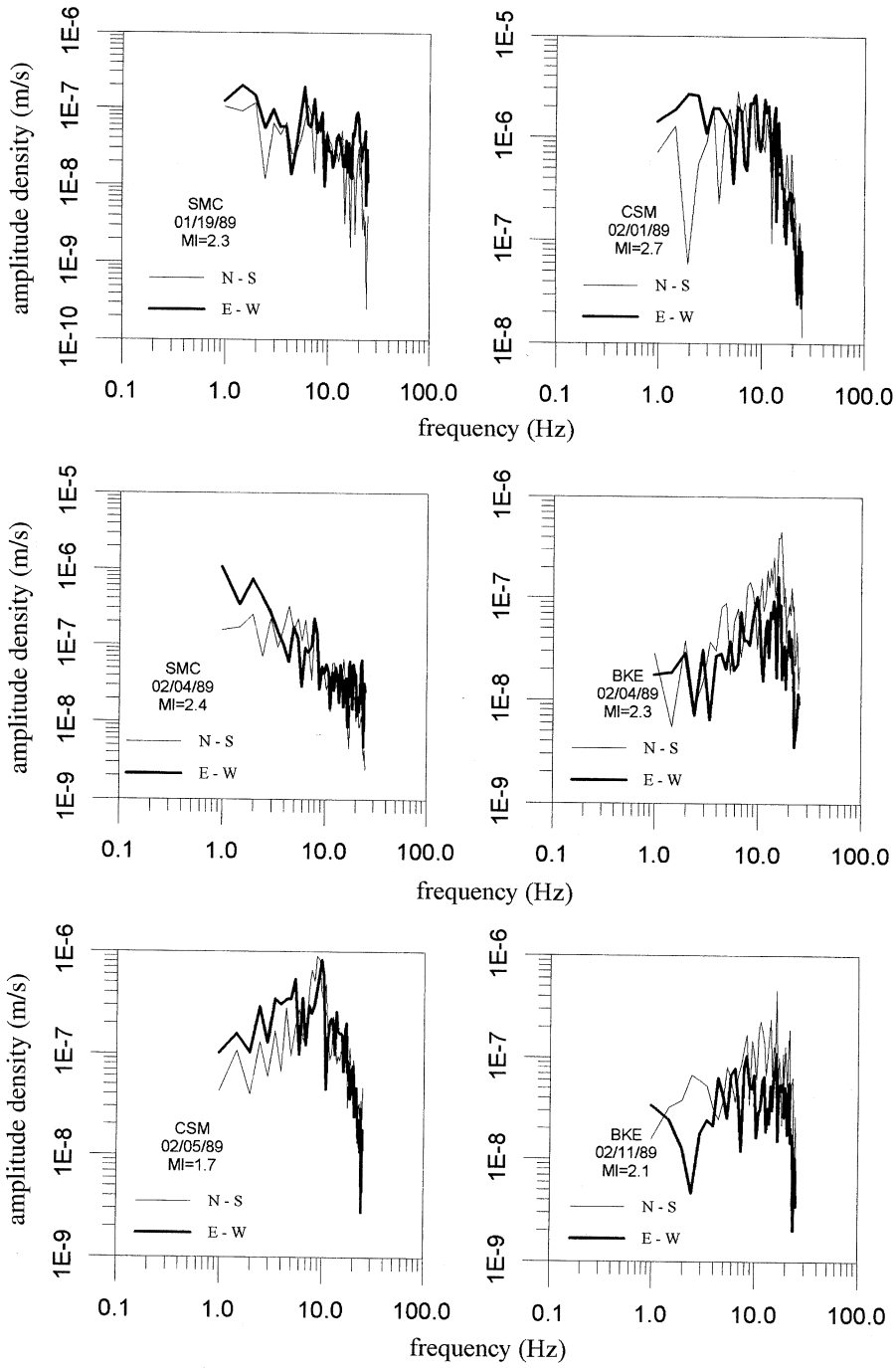

Fig. 6a. Amplitude displacement spectra of the horizontal components of analyzed events for 1989 swarm.

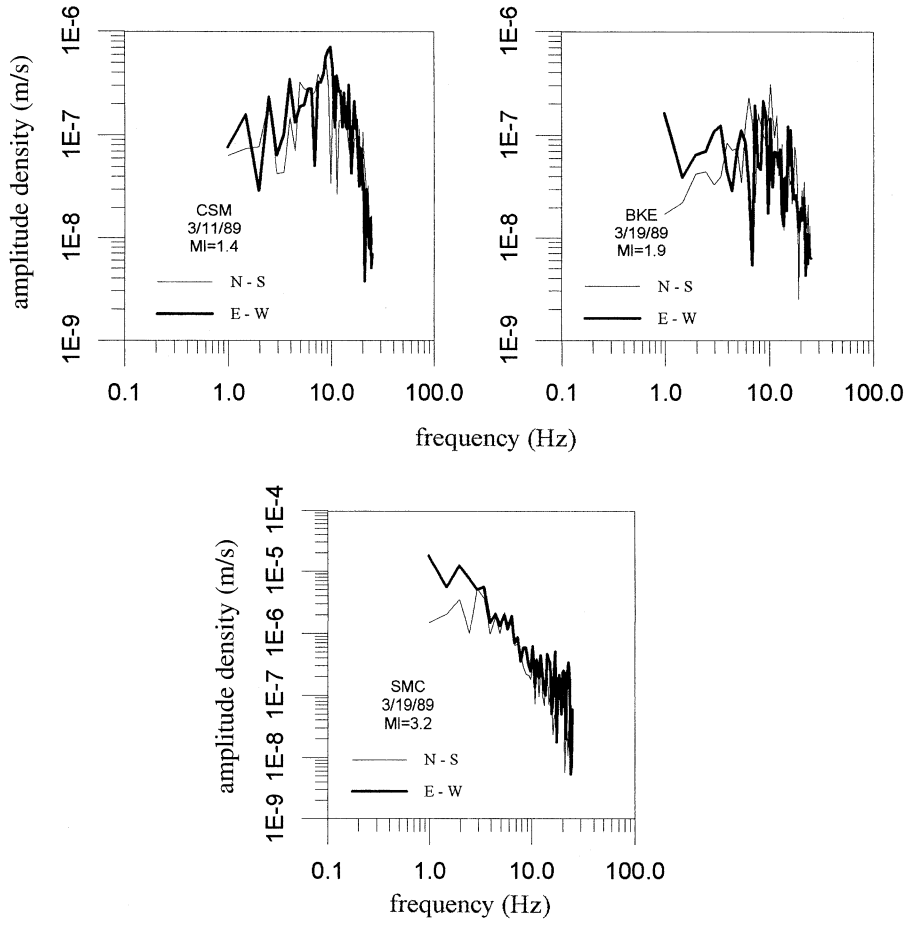

Fig. 6a. (*continued*).

anisms for the two swarm episodes, nor with respect to the normal seismicity of the volcano. Focal mechanisms are dominantly strike slip, with a small occurrence of normal or thrust fault components. No clear pattern is evident for the principal P and T axes, which often appear reversed from one earthquake to another.

4. Spectral analyses of the largest events

Data from the digital stations allows us to study spectral content and acceleration levels for the largest events. This is a key question, not yet addressed till now, in view of the importance of the evaluation of seismic hazard and risk related to volcano unrest episodes. We have computed displacement and acceleration spectra for the analyzed events, and accelerograms for the largest magnitude events, at the digital three component stations. Amplitude spectra were computed by Fast Fourier Transform. In order to obtain accelerograms, FFT were applied to recorded velocity traces; then, Fourier Transforms were multiplied by $i\omega$, and the inverse transform used to return in the time do-

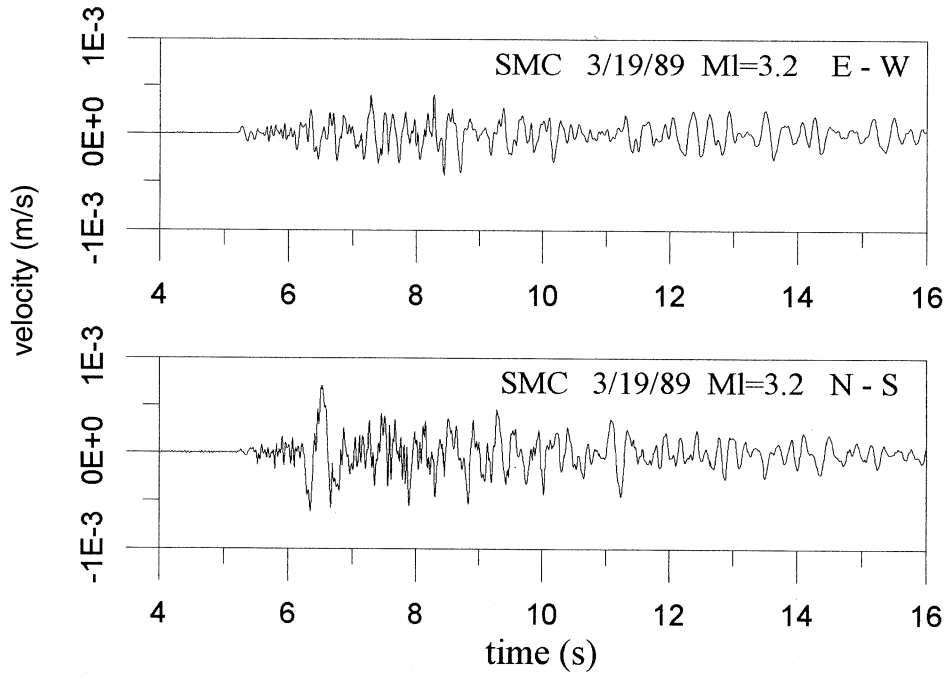

Fig. 6b. The horizontal components for one of the largest events, namely the M_L = 3.2 (89/03/19 one), as recorded at the station SMC.

main. Some amplitude displacement spectra of the horizontal components of analyzed events are shown in figs. 6a and fig. 7 for 1989 and 1995 swarm, respectively. Figure 6b also reports the horizontal component seismogram for one of the largest events (the M_L = 3.2, 3/19/89), as recorded at the station SMC. These plots, show very high peak amplitudes, at about 10-15 Hz, for the stations BKE, BKS and CSM. Station SMC does not show such pronounced effects. This large distortions of the amplitude spectra hide the corner frequencies, preventing the estimation of characteristic source dimensions. The peak frequency, almost stable for various stations and various earthquakes, is likely to reflect some particular propagation effect, probably over a path common to the seismic rays recorded at the sites BKE, BKS and CSM. As visible in fig. 2, the most striking structural difference among the sites of BKE, BKS and CSM on one side, and SMC on the other, is that the first group is located on the younger structure of Vesuvius, while SMC is located on the ancient Somma structure.

The largest recorded events at Somma-Vesuvius occurred during the 1989 and 1995 crises. Maximum recorded magnitudes range between 3.0 and 3.4, and, in the considered periods some of the largest events occurred, with magnitudes between 3.1 and 3.2.

Accelerograms and spectra for the three largest events, namely the 3/19/89 (M_L = 3.2), 9/16/95 (M_L = 3.2) and 9/24/95 (M_L = 3.1) are shown in fig. 8. Peak accelerations show high differences in site amplification. In particular, there is a dramatic difference, of more than one order of magnitude, between the peak accelerations for the 3/19/89 event as recorded at CSM and SMC. Peak accelerations at CSM reach values of 0.7 m s^{-2}, corresponding to 0.06 times the gravity acceleration, which is an extremely high value for an event of magnitude 3.2.

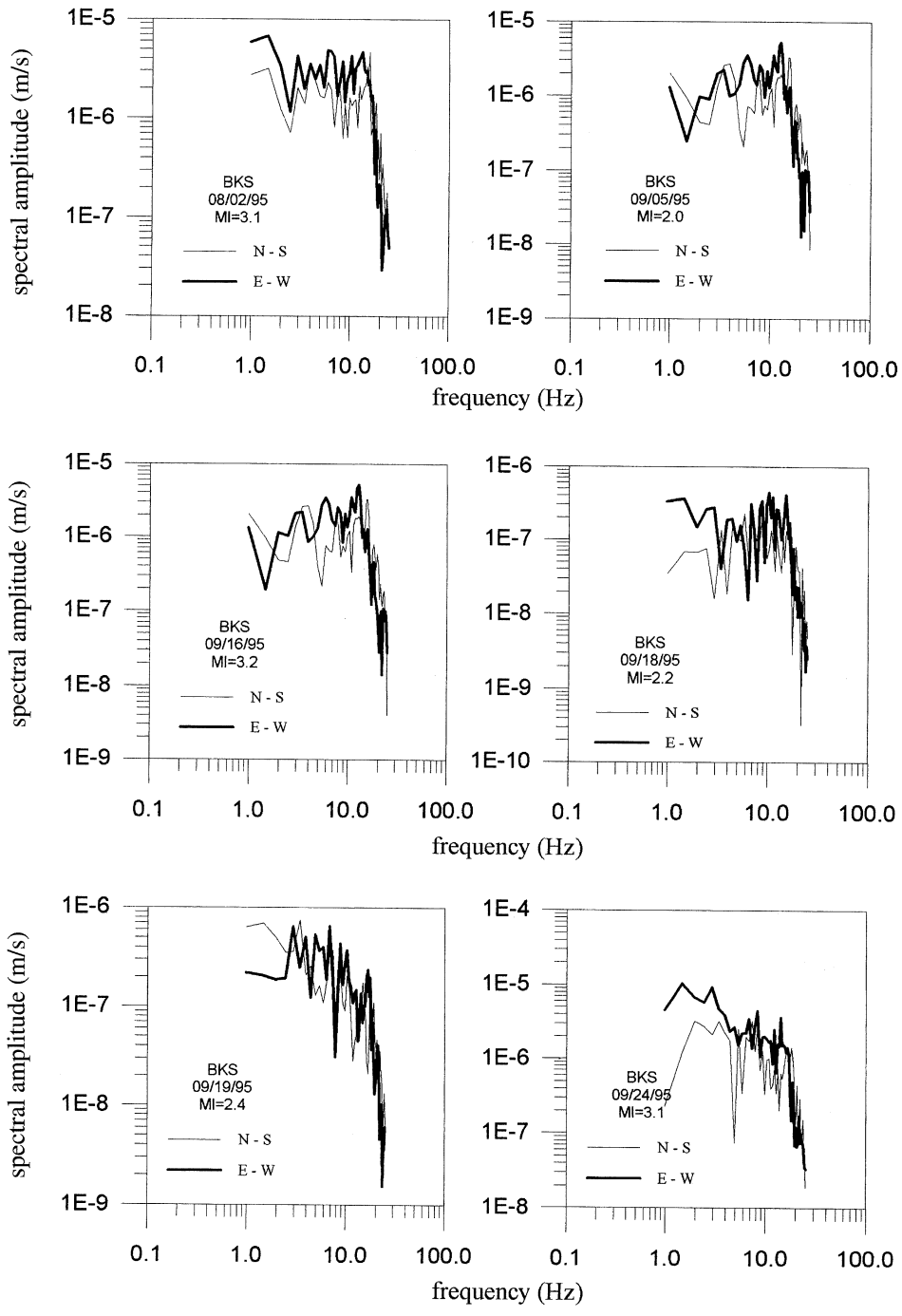

Fig. 7. Amplitude displacement spectra of the horizontal components of analyzed events for 1995.

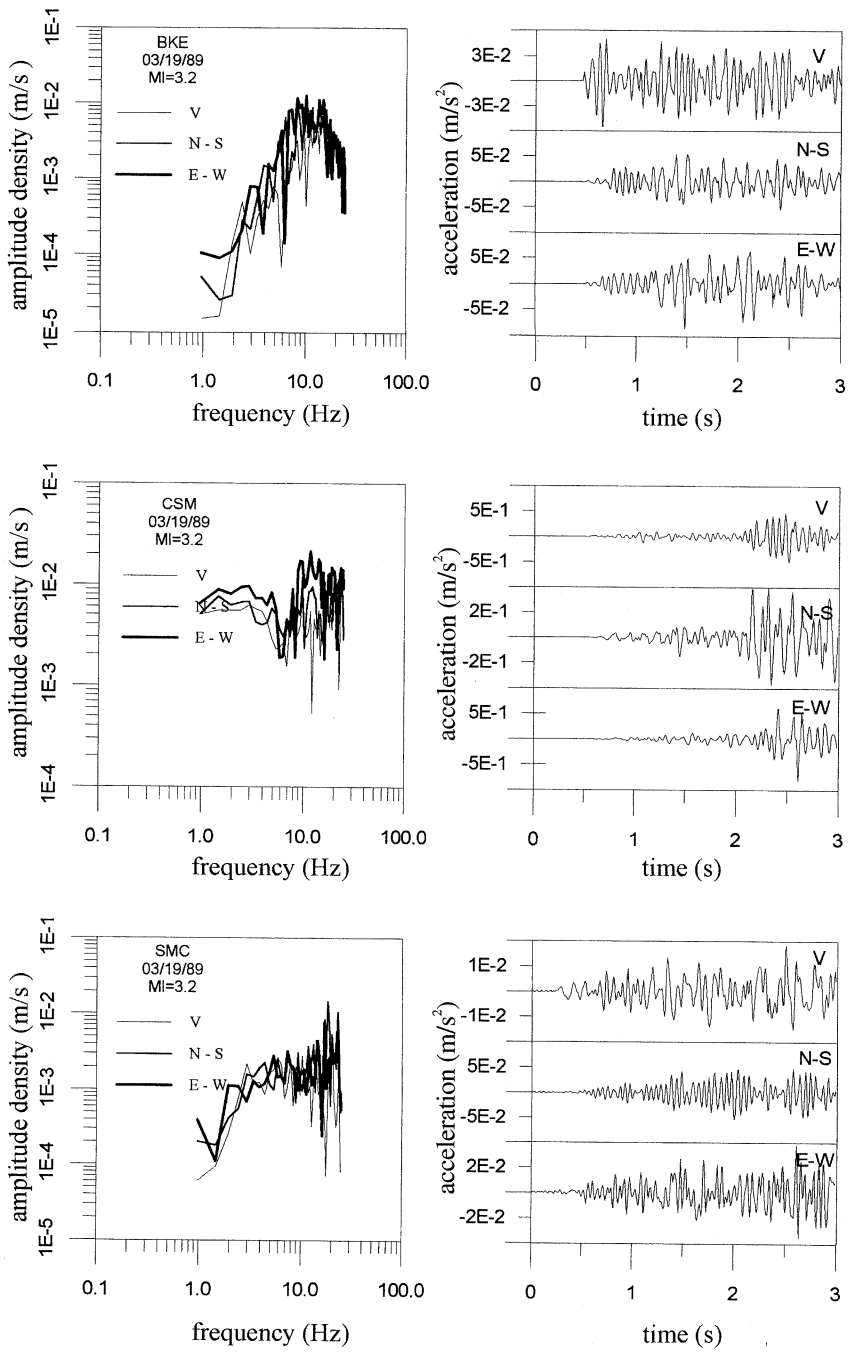

Fig. 8. Accelerograms and acceleration spectra for the three largest events, namely the 3/19/89 (M_L = 3.2), 9/16/95 (M_L = 3.2) and 9/24/95 (M_L = 3.1). Peak accelerations show high differences in site amplification.

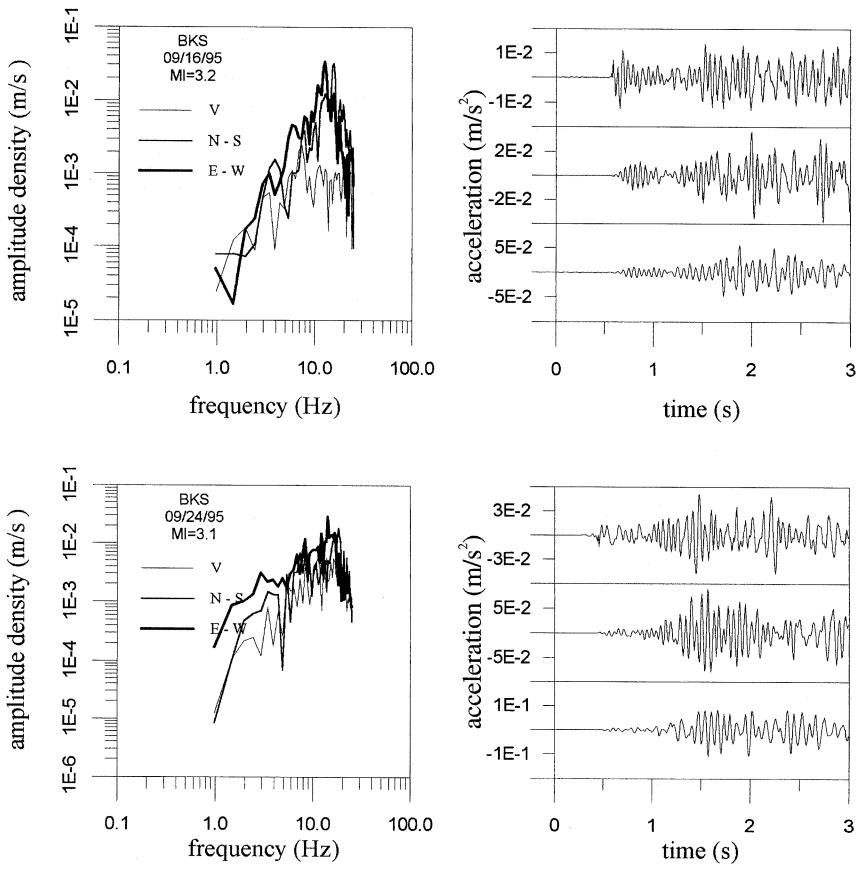

Fig. 8. (*continued*).

5. Discussion and conclusions

Some microearthquakes which occurred at Somma-Vesuvius during two swarm episodes in 1989 and 1995 have been analyzed. In both periods, some events of magnitude $M_L > 3$ occurred, corresponding to the highest magnitudes of Somma-Vesuvius local earthquakes. The earthquakes which occurred in 1989 were recorded by a limited number of stations, including four digital, three component stations of a mobile network, thus making problematic the estimate of focal mechanisms. However, using the probability method developed by De Natale *et al.* (1991), with joint use of *P* polarities, *S* polarizations and, sometimes, *S/P* amplitude ratios, we managed to obtain reliable mechanisms also for small earthquakes recorded by less than six stations.

The analyzed earthquakes occurred very close to the crater axis of Mt. Vesuvius, where most of the seismicity is located, at depths ranging between 1 and 6 km bsl. Focal mechanisms of such earthquakes are dominantly strike-slip, with minor normal or thrust components. No evident regularities can be seen for the distribution of *P*- and *T*-axes, which often appears opposite for different events. Overall, no significant differences among the events of the two swarm episodes exist, even with seismicity occurring dur-

ing periods of normal background seismicity (Vilardo *et al.*, 1996). The occurrence of local seismicity close to the crater axis, with irregular distribution of mechanism axes, is probably due to the presence of a high velocity anomaly zone, as evidenced by seismic tomography (Zollo *et al.*, 1996), interpreted as the high rigidity inner core of the volcano, which concentrates at its border stresses produced by regional and local (gravitative load) stress. The joint effect of such structure and the gravitative loading produces a state of stress, which can reach orders of magnitudes of some MPa, very close to the critical rupture threshold (De Natale *et al.*, 1999).

In this paper we analyzed four $M_L > 3.0$ events which occurred in 1989 and 1995. We determined displacement and acceleration spectra for all the digital recordings of studied earthquakes, and accelerograms for the four highest magnitude events. We evidenced that stations located on the youngest Vesuvius structure are characterized by strong spectral amplifications between 10 and 15 Hz. Such spectral peaks, observed for all the events, are likely to represent propagation effects linked to the Vesuvius structure or high attenuation of higher frequencies for ray path travelling through Mt. Somma. The only station located on the older Somma structure does not show such effect on earthquake spectra, or, at least, not of such amplitude. Ground accelerations for the highest events were computed from velocity time series by derivation in the frequency domain. Observed values of peak ground accelerations range from 0.02 m s^{-2} to 0.7 m s^{-2}. The highest value was observed to the station CSM for the largest event (M_L = 3.2) of the 19/03/1989 sequence. Peak accelerations of the same event at the other stations are about one order of magnitude smaller, thus suggesting that such an anomalously high value recorded at CSM reflects local amplification effects. Looking at the acceleration spectra of fig. 8, it appears that a major peculiarity of CSM is the high amplification of low frequencies, in the range 1-10 Hz, with respect to the other stations. Furthermore, ground accelerations computed for other events, confirm the existence of a local amplification effect at CSM, causing peak accelerations about one order of magnitude larger.

In conclusion, this paper presents a first attempt to evaluate the features of seismicity occurring at Somma-Vesuvius during swarm periods. It appears that seismicity in such periods has almost the same features as in normal periods, except for a larger rate in seismic energy, and larger absolute magnitudes. Furthermore, this paper presents a first attempt to evaluate the ground motion produced by local earthquakes, as related to local site amplifications. The large evidenced site effects call for a large effort to be made, in the future, for detailed analyses of this subject, crucial for a correct understanding of seismic hazard in such a densely populated area.

Acknowledgements

We gratefully appreciate the thoughtful and constructive comments of Claudio Chiarabba. This paper was partially supported by a GNV-CNR contract.

REFERENCES

BERRINO, G., U. COPPA, G. DE NATALE and F. PINGUE (1993): Recent geophysical investigations at Somma-Vesuvius volcanic complex, *J. Volcanol. Geotherm. Res.*, **58**, 239-262.

CASSANO, E. and P. LA TORRE (1987): Geophysics in Somma-Vesuvius, in *Quad. Ric. Sci.*, edited by R. SANTACROCE, CNR, Roma, 175-196.

DE NATALE, G., (1994): Focal mechanism determination for volcanic microearthquakes, *Ann. Geofis.*, **37** (6), 1621-1643.

DE NATALE, G., A. FERRARO and J. VIRIEUX (1991): A probability method for earthquakes focal mechanism, *Geophys. Res. Lett.*, **18**, 1-4.

DE NATALE, G., P. CAPUANO, C. TROISE and A. ZOLLO (1998): Seismicity at Somma-Vesuvius and its implications for the 3D tomography of the volcano, *J. Volcanol. Geotherm. Res.*, **82**, 175-197.

DE NATALE, G., S.M. PETRAZZUOLI, C. TROISE, F. PINGUE and P. CAPUANO (1999): Internal stress field at Mt.Vesuvius as due to gravitative and structural effect: a model for the generation of background seismicity at a central volcano, *Geophys. Res. Lett.* (submitted).

FERRUCCI, F., G. GAUDIOSI, N.A. PINO, G. LUONGO, A. HIRN and L. MIRABILE (1989): Seismic detection of a major Moho upheaval beneath the Campania volcanic area (Naples, Southern Italy), *Geophys. Res. Lett.*, **16**, 1317-1320

FINETTI, I. and C. MORELLI (1974): Esplorazione di sismica a riflessione dei Golfi di Napoli e Pozzuoli, *Boll. Geofis. Teor. Appl.*, **16**, 175-222.

PRINCIPE, C., M. ROSI, R. SANTACROCE and A. SBRANA (1987): Explanatory notes to the geological map in Somma-Vesuvius, in *Quad. Ric. Sci., e*dited by R. SANTACROCE, CNR, Roma, 11-52.

THURBER, C.H. (1983): Earthquakes locations and three dimensional crustal structure in the Coyote Lake area, Central California, *J. Geophys. Res.,* **88**, 8226-8236.

VILARDO, G., G. DE NATALE, G. MILANO and U. COPPA (1996): The seismicity of Mt. Vesuvius, *Tectonophysics,* **261**, 127-138.

ZOLLO, A., and P. BERNARD (1991): Fault mechanism for near source data: joint inversion of *P* polarities and *S* polarizations, *Geophys. J. Int.*, **104**, 441-452.

ZOLLO, A., P. GASPARINI, J. VIRIEUX, H. LE MEUR, G. DE NATALE, G. BIELLA, E. BOSCHI, P. CAPUANO, R. DE FRANCO. P. DELL'AVERSANA, R. DE MATTEIS, I. GUERRA, G. IANNACCONE, L. MIRABILE and G. VILARDO (1996): Seismic evidence for a low velocity zone in the upper crust beneath Mount Vesuvius, *Science*, **274**, 592-594.

ZOLLO, A., P. GASPARINI, J. VIRIEUX, G. BIELLA, E. BOSCHI, P. CAPUANO, R. DE FRANCO, P. DEL-L'AVERSANA, R. DE MATTEIS, G. DE NATALE, G. IANNACCONE, I. GUERRA, H. LE MEUR and L. MIRABILE (1998): An image of Mt. Vesuvius obtained by 2D seismic tomography, *J. Volcanol. Geotherm. Res.,* **82**, 161-173.